

**ARTICLE****Robust Variable-Pitch Control Design of PMSG Via Perturbation Observer**Yilin Hu¹, Yan Xie², Bo Li^{3,*}, Yiqiang Jiang¹ and Fu Bao¹¹Department of International Applied Technology, Yibin University, Yibin, 644000, China²School of Information and Communication Engineering, Hainan University, Haikou, 570000, China³School of Physics and Information Engineering, Zhaotong University, Zhaotong, 657000, China

*Corresponding Author: Bo Li. Email: 20192205026@stu.kust.edu.cn

Received: 27 October 2020 Accepted: 15 November 2020

ABSTRACT

Wind turbine employs pitch angle control to maintain captured power at its rated value when the wind speed is higher than rated value. This work adopts a perturbation observer based sliding-mode control (POSMC) strategy to realize robust variable-pitch control of permanent magnet synchronous generator (PMSG). POSMC combines system nonlinearities, parametric uncertainties, unmodelled dynamics, and time-varying external disturbances into a perturbation, which aims to estimate the perturbation via a perturbation observer without an accurate system model. Subsequently, sliding mode control (SMC) is designed to completely compensate perturbation estimation in real-time for the sake of achieving a global consistent control performance and improving system robustness under complicated environments. Simulation results indicate that, compared with vector control (VC), feedback linearization control (FLC), and nonlinear adaptive control (NAC), POSMC has the best control performance in ramp wind and random wind and the highest robustness in terms of parameter uncertainty. Specially, the integral absolute error index of ω_m of POSMC is only 11.69%, 12.10% and 15.14% of that of VC, FLC and NAC in random wind speed.

KEYWORDS

Variable-pitch control; permanent magnet synchronous generator; perturbation observer

1 Introduction

Energy is an essential material basis and support for human survival and social-economic development [1]. However, extensive consumption of limited fossil energy sources such as coal, oil, and natural [2] lead to severe environmental pollution, greenhouse effect, and increased global warming which are the common challenges in the world [3]. Hence, develop various renewable energy, e.g., wind [4], solar [5], geothermal [6], tides [7], waves [8], etc., and improve its efficiency have become a global consensus [9]. Specially, wind energy is one of promising alternative energy with the merits of pollution-free, cheap, widespread, and unlimited supply [10]. According to statistics of Renewables 2020 Global Status Report, the total growth rate of wind power capacity is around 228.79% in the globe over the past decade, which leads to a total of 651 GW installation up to 2019 [11].

Currently, permanent magnet synchronous generator (PMSG) is an attractive choice of wind turbine (WT) due to its large thrust, low loss, high-efficiency density, and high energy conversion efficiency [12].



And the operating regions of PMSG can be divided into three parts, as shown in Fig. 1. Specially, in Region 2, wind speed is between cut-in wind speed and rated value. The task of WT is to control turbine speed at the optimal value for extracting the maximum output power [13]. In Region 3, wind speed is between rated value and cut-out wind speed. The variable pitch controller adjusts the blade pitch angle to maintain output power at its rated value as the capacities of generator and converter are limited [14].

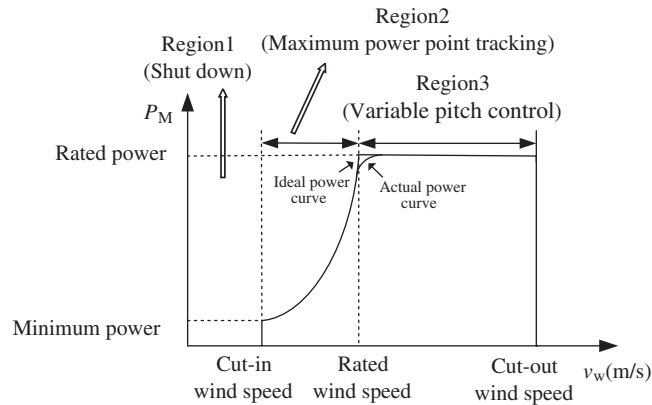


Figure 1: Three operating regions of PMSG

Various variable pitch control techniques have been reported in publications during the past decades so far. Conventional vector control (VC) using proportional-integral (PI) and proportional-integral-derivative (PID) control are widely adopted in industrial processes owing to its strengths of simple configuration and convenient implementation [15]. Nevertheless, it is an approximated linearization model based on an equilibrium point in which performance will inevitably degrade when the operating point is changed [16]. The linear quadratic Gaussian (LQG) is another common method in pitch angle control which can provide high robustness in terms of the phase and gain margins [17]. Nevertheless, wind energy conversion systems (WECS) are highly nonlinear due to the randomness, intermittence, and seasons of wind energy such that this linear controller only has poor performance [18]. Hence, a series of advanced control strategies for pitch angle control, e.g., nonlinear control, fuzzy control, robust control, and self-adaptive control are presented to overcome the defects of VC and LQG. Adaptive PID [19] control and fuzzy self-tuning PID control [20] tune PID parameters on-line, which can suppress a variety of nonlinear, time-varying factors. But the inherent drawback of PID is still retained in the above frameworks, which cannot obtain consistent control performance [21]. Moreover, Senjyu et al. [22] proposes a generalized predictive control (GPC) for wind generators in all operating regions which can effectively mitigate the adverse effects of changed operating points. Van et al. [23] develops a low-cost fuzzy logic controller for variable-speed WT without consideration of expensive wind speed measurements. And Wang et al. [24] designs a two-degree-of-freedom motion mechanism with feedback linearization control (FLC) for the large WT with improved robustness and stability. Moreover, multi-layer perceptron and radial basis function neural networks are investigated in work [25] to prevent WT from overloading or shutting down during high wind speed. Recently, perturbation observer has been applied widely in nonlinear system control, such as WECS [26], photovoltaic systems [27], VSC-HVDC systems [28] and so on, which can on-line estimate unknown nonlinearities, parametric uncertainties, and time-varying external disturbances for nonlinear system without the requirement of detailed system model [29].

In this work, a perturbation observer based sliding-mode control (POSMC) is adopted for PMSG to limit the turbine output power and generator speed in Region 3. Firstly, the perturbation observer generates the new perturbation via combining the system nonlinearities, parametric uncertainties, unmodelled

dynamics, and time-varying external disturbances. Then sliding mode control is utilized to completely compensate the perturbation estimation in real-time. The proposed POSMC retains the strong robustness of sliding-mode control (SMC), and only require the measurements of d-q axis current and mechanical rotation speed. Three case studies are studied by Matlab/Simulink, e.g., ramp wind speed, random wind speed, and parameter uncertainty. Simulation results validate that, compared with VC control, feedback linearization control (FLC) and nonlinear adaptive control (NAC), POSMC can achieve satisfactory robust control performance under various operating conditions.

The rest of this article is organized as follows: Section 2 gives the model of PMSG system; Section 3 introduces the theory of POSMC; Section 4 develops the detailed design of POSMC for variable-pitch PMSG. In Section 5, case studies results are discussed and analyzed. And the last Section summarizes this work and draws conclusions.

2 Modelling of PMSG System

A representative topology of PMSG system is described in Fig. 2. Firstly, mechanical power is transformed into electrical power via WT. Then, the electrical power is injected into power grid through back-to-back voltage source converters, filters, and the transformer. Specially, the major task of the machine-side converter (MSC) is to capture mechanical power and provide the required stator voltage, while active power and reactive power are regulated by the grid-side converter (GSC) [30]. In addition, MSC and GSC can realize a fully decoupled control by the DC link.

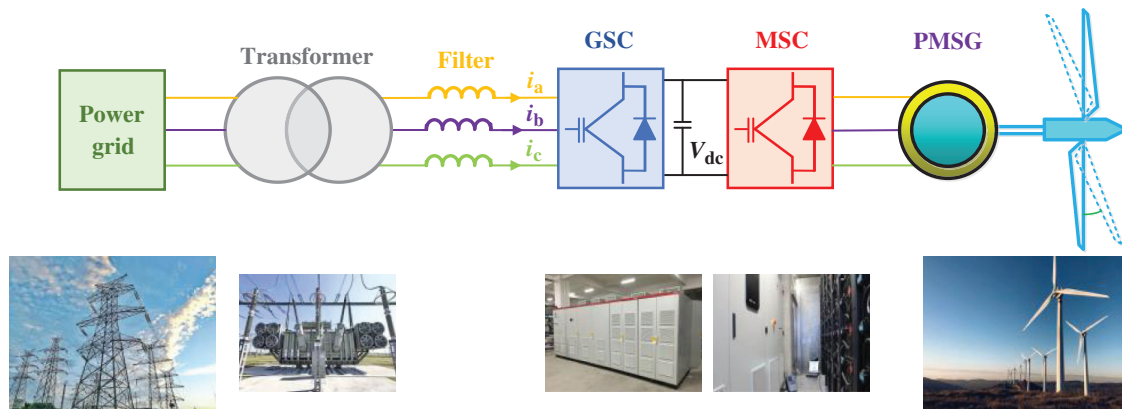


Figure 2: A representative topology of PMSG system

2.1 WT Model

The tip speed ratio λ of WT is denoted as [15]

$$\lambda = \frac{R\omega_m}{V} \tag{1}$$

where R represents the blade radius, ω_m is the mechanical rotation speed, V is the wind speed.

According to aerodynamic theory, the electrical power extracted by the WT can be described as

$$P_m = \frac{1}{2} \rho \pi R^2 V^3 C_p(\beta, \lambda) \tag{2}$$

where ρ is the air density. And the power coefficient $C_p(\beta, \lambda)$ can be represented by pitch angle β and λ

$$C_p = 0.22 \left(\frac{116}{\lambda_i} - 0.4\beta - 5 \right) e^{\frac{-12.5}{\lambda_i}} \quad (3)$$

$$\frac{1}{\lambda_i} = \frac{1}{\lambda + 0.08\beta} - \frac{0.035}{\beta^3 + 1} \quad (4)$$

2.2 Generator System Model

The voltage and torque equations of PMSG can be denoted as

$$V_d = i_d R_s + L_d \frac{di_d}{dt} - \omega_e L_q i_q \quad (5)$$

$$V_q = i_q R_s + L_q \frac{di_q}{dt} + \omega_e (L_d i_d + K_e) \quad (6)$$

$$T_e = p [(L_d - L_q) i_d i_q + i_q K_e] \quad (7)$$

where V_d and V_q represent d-q axis stator voltages, i_d and i_q are d-q axis stator currents, L_d and L_q are d-q axis inductances, $\omega_e = p\omega_m$ is electrical rotate-speed, T_e is the electromagnetic torque, p is the number of pole pairs, and K_e is the permanent magnetic flux.

2.3 Drive Train Model

The dynamics model of mechanical shaft system can be represented by

$$J_{\text{tot}} \frac{d\omega_m}{dt} = T_m - T_e \quad (8)$$

$$T_m = \frac{1}{2} \rho \pi R^5 \frac{C_p(\lambda, \beta)}{\lambda^3} \omega_m^2 \quad (9)$$

where J_{tot} denote the total inertia of the drive train, T_m is the mechanical torque, D is the viscous damping coefficient. Note that T_e has a much faster response than T_m , thus let $\dot{T}_e = 0$ in this paper to realize simplified calculation.

2.4 Pitch Angel Control Model

Pitch angel control actuator could regulate the blade pitch based on the required value. And the first-order linear model of pitch angel control actuator without considering the delay characteristics can be given as [14]

$$\dot{\beta} = -\frac{\beta}{\tau_\beta} + \frac{\beta_r}{\tau_\beta} \quad (10)$$

where β_r is the required pitch angle, and τ_β is the time constant of actuator.

3 Perturbation Observer Based Sliding-Mode Control

3.1 Design of SMSPO

An uncertain nonlinear system is denoted as

$$\begin{cases} \dot{x} = Ax + B(a(x) + b(x)u + d(t)) \\ y = x_1 \end{cases} \quad (11)$$

where $x = [x_1, x_2, \dots, x_n]^T \in \mathbb{R}^n$, $u \in \mathbb{R}$, $y \in \mathbb{R}$ denote state vector, control input, and system output, respectively. $a(x) : \mathbb{R}^n \mapsto \mathbb{R}$ and $b(x) : \mathbb{R}^n \mapsto \mathbb{R}$ represent unknown smooth functions, and $d(t) : \mathbb{R}^+ \mapsto \mathbb{R}$ is time-varying external disturbance.

The perturbation of system (11) is described as

$$\psi(x, u, t) = a(x) + (b(x) - b_0)u + d(t) \tag{12}$$

where b_0 is constant control gain.

Based on Eq. (12), the last state x_n of system (11) is represented as

$$\dot{x}_n = a(x) + (b(x) - b_0)u + d(t) + b_0u = \psi(x, u, t) + b_0u \tag{13}$$

Define a fictitious state x_{n+1} to denote perturbation $\psi(x, u, t)$, then the original n th order system can be extended into the $(n+1)$ th order augmented system, yields

$$\begin{cases} y = x_1 \\ \dot{x}_1 = x_2 \\ \vdots \\ \dot{x}_n = x_{n+1} + b_0u \\ \dot{x}_{n+1} = \psi(\cdot) \end{cases} \tag{14}$$

Define the extended state vector $x_{\text{extend}} = [x_1, x_2, \dots, x_n, x_{n+1}]^T$, and propose the assumptions:

Assumption 1: b_0 is selected to meet $|b(x)/b_0 - 1| \leq \theta < 1$, where θ represents a positive constant.

Assumption 2: perturbation $\psi(x, u, t)$ and its derivative $\dot{\psi}(x, u, t)$ are bonded within the domain: $|\psi(x, u, t)| \leq \gamma_1$, $|\dot{\psi}(x, u, t)| \leq \gamma_2$ with $\psi(0, 0, 0) = 0$ and $\dot{\psi}(0, 0, 0) = 0$, where γ_1 and γ_2 are positive constants.

Suppose $y = x_1$ is the sole measurable state, a $(n+1)$ th order SMSPO is designed to estimate the system states and perturbation, obtains

$$\begin{cases} \dot{\hat{x}}_1 = \hat{x}_2 + \alpha_1 \tilde{x}_1 + k_1 \text{sat}(\tilde{x}_1) \\ \vdots \\ \dot{\hat{x}}_n = \hat{\psi}(\cdot) + \alpha_n \tilde{x}_1 + k_n \text{sat}(\tilde{x}_1) + b_0u \\ \dot{\hat{\psi}}(\cdot) = \alpha_{n+1} \tilde{x}_1 + k_{n+1} \text{sat}(\tilde{x}_1) \end{cases} \tag{15}$$

where \hat{x} represents the estimated value of x , $\tilde{x} = x - \hat{x}$ denotes the estimation error, positive constants α_i ($i = 1, 2, \dots, n$) are observer gains, and positive constants k_i ($i = 1, 2, \dots, n$) are sliding surface gains.

3.2 Design of Sliding-Mode Controller

An estimated sliding surface is defined as

$$\hat{S}(x, t) = \sum_{i=1}^n \rho_i (\hat{x}_i - y_d^{(i-1)}) \tag{16}$$

where the estimated sliding surface gains $\rho_i = C_{n-1}^{i-1} \lambda_c^{n-i}$ ($i = 1, 2, \dots, n$) place all the poles of estimated sliding surface on the left half $-\lambda_c$ of complex plane with $\lambda_c > 0$.

Finally, POSMC of system is given as

$$u = \frac{1}{b_0} \left[y_d^{(n)} - \sum_{i=1}^{n-1} \rho_i (\hat{x}_{i+1} - y_d^{(i)}) - \varsigma \hat{S} - \varphi \text{sat}(\hat{S}, \delta_c) - \hat{\psi}(\cdot) \right] \quad (17)$$

where ς and φ are controller gains, δ_c is the thickness layer boundary of controller.

4 POSMC Design of Variable-Pitch PMSG

4.1 State-Space Equation of PMSG

The state-space equation of PMSG is represented by

$$\dot{x} = f(x) + g_1(x)u_1 + g_2(x)u_2 + g_3(x)u_3 \quad (18)$$

where

$$f(x) = \begin{bmatrix} -\frac{\beta}{\tau_\beta} \\ -\frac{R_s}{L_d} i_d + \frac{\omega_e L_q}{L_d} i_q \\ -\frac{R_s}{L_q} i_q - \frac{1}{L_q} \omega_e (L_d i_d + K_e) \\ \frac{1}{J_{\text{tot}}} T_m \end{bmatrix} \quad (19)$$

$$g(x) = \begin{bmatrix} -\frac{\beta}{\tau_\beta} & 0 & 0 & 0 \\ 0 & \frac{1}{L_d} & 0 & 0 \\ 0 & 0 & \frac{1}{L_q} & 0 \\ 0 & 0 & 0 & 0 \end{bmatrix} \quad (20)$$

$$x = [\beta \quad i_d \quad i_q \quad \omega_m]^T \quad (21)$$

$$u = [u_1, u_2, u_3]^T = [\beta_r, V_d, V_q]^T \quad (22)$$

$$y = [y_1, y_2, y_3]^T = [h_1(x), h_2(x), h_3(x)]^T = [\omega_m, i_d, i_q]^T \quad (23)$$

where $x \in R^4$, $u \in R^3$, and $y \in R^3$ are state vector, control input, and system output, respectively. R_s is the stator resistance, V_d and V_q are d-q axis stator voltages, and $\omega_e = p\omega_m$ is the electrical generator rotation speed.

4.2 Pitch Angle Control

Differentiate control output $y_1 = \omega_m$ until it appears explicitly, as

$$\begin{aligned} \ddot{y}_1 = \frac{1}{J_{\text{tot}}} \dot{T}_m = & A \left(-\frac{C_p}{\omega_m} - \frac{RV}{F^2} E \right) \frac{d\omega_m}{dt} - \frac{AE\beta}{\tau_\beta} \left[-\frac{0.088e^{-12.5\tau}}{E} - \frac{0.08V^2}{F^2} + \frac{0.105\beta^2}{(1+\beta^3)^2} \right] \\ & + \frac{AE}{\tau_\beta} \left[-\frac{0.088e^{-12.5\tau}}{E} - \frac{0.08V^2}{F^2} + \frac{0.105\beta^2}{(1+\beta^3)^2} \right] u_1 \end{aligned} \quad (24)$$

where

$$A = \frac{\rho\pi R^2 V^3}{2\omega_m} \quad (25)$$

$$E = (39.27 - 319\tau + 1.1\beta)e^{-12.5\tau} \quad (26)$$

$$F = \omega_m R + 0.08\beta V \quad (27)$$

$$\tau = \frac{1}{\lambda + 0.08\beta} - \frac{0.035}{\beta^3 + 1} \quad (28)$$

Eq. (24) can be rewritten into matrix form, yields

$$\ddot{y}_1 = F_1(x) + B_1(x)u_1 \quad (29)$$

where

$$F_1(x) = A \left(-\frac{C_p}{\omega_m} - \frac{RV}{F^2} E \right) \frac{d\omega_m}{dt} - \frac{AE\beta}{\tau_\beta} \left[-\frac{0.088e^{-12.5\tau}}{E} - \frac{0.08V^2}{F^2} + \frac{0.105\beta^2}{(1 + \beta^3)^2} \right] \quad (30)$$

$$B_1(x) = \frac{AE}{\tau_\beta} \left[-\frac{0.088e^{-12.5\tau}}{E} - \frac{0.08V^2}{F^2} + \frac{0.105\beta^2}{(1 + \beta^3)^2} \right] \quad (31)$$

Note that $\det[B_1(x)] \neq 0$ when $V \neq 0$ and $\beta \neq 0$, thus $B_1(x)$ is nonsingular in all the feasible zone. In other words, above input-output linearization is valid.

Define perturbation $\psi_1(\cdot)$ to describe the nonlinearities and uncertainties of $F_1(x)$ and $B_1(x)$, yields

$$\psi_1(\cdot) = F_1(x) + (B_1(x) - B_1(0))u_1 \quad (32)$$

where $B_1(0) = b_{10}$ is constant control gain.

Define tracking error $e_1 = [\omega_m - \omega_m^*]$ where ω_m^* is the reference of ω_m , one can obtain

$$\ddot{e}_1 = \psi_1(\cdot) + B_1(0)u_1 - \ddot{\omega}_m^* \quad (33)$$

Then, a third order sliding-mode state and perturbation observer (SMSPO) is adopted to estimate $\psi_1(\cdot)$, as

$$\begin{cases} \dot{\tilde{\omega}}_m = \hat{\omega}_m + \alpha_{11}\tilde{\omega}_m + k_{11}\text{sat}(\tilde{\omega}_m, \delta_o) \\ \dot{\hat{\omega}}_m = \hat{\psi}_1(\cdot) + \alpha_{12}\tilde{\omega}_m + k_{12}\text{sat}(\tilde{\omega}_m, \delta_o) + B_1(0)u_1 \\ \dot{\hat{\psi}}_1(\cdot) = \alpha_{13}\tilde{\omega}_m + k_{13}\text{sat}(\tilde{\omega}_m, \delta_o) \end{cases} \quad (34)$$

where positive constants α_{11} , α_{12} , α_{13} , k_{11} , k_{12} , and k_{13} are observer gains.

The estimated sliding surface of system (29) is chosen as

$$\hat{S}_1 = \rho_1(\hat{\omega}_m - \omega_m^*) + \rho_2(\dot{\hat{\omega}}_m - \dot{\omega}_m^*) \quad (35)$$

Finally, the POSMC of system (29) is designed as

$$u_1 = \frac{1}{B_1(0)} \left[\ddot{\omega}_m^* - \rho_1(\dot{\hat{\omega}}_m - \dot{\omega}_m^*) - \varsigma_1 \hat{S}_1 - \varphi_1 \text{sat}(\hat{S}_1, \delta_c) - \hat{\psi}_1(\cdot) \right] \quad (36)$$

where ρ_1 is estimated sliding surface gains, ς_1 and φ_1 are controller gains.

4.3 Generator Control

Differentiate control output $y = [y_2, y_3]^T = [i_d, i_q]^T$ until it appears explicitly, as

$$\begin{bmatrix} \dot{y}_2 \\ \dot{y}_3 \end{bmatrix} = \begin{bmatrix} F_2(x) \\ F_3(x) \end{bmatrix} + B_2(x) \begin{bmatrix} u_2 \\ u_3 \end{bmatrix} \quad (37)$$

where

$$F_2(x) = \frac{1}{L_d} (-i_d R_s + \omega_e L_q i_q) \quad (38)$$

$$F_3(x) = -\frac{R_s}{L_q} i_q + \frac{1}{L_q} \omega_e (L_d i_d + k_e) \quad (39)$$

$$B_2(x) = \begin{bmatrix} B_{21} & B_{22} \\ B_{23} & B_{24} \end{bmatrix} = \begin{bmatrix} \frac{1}{L_d} & 0 \\ 0 & \frac{1}{L_q} \end{bmatrix} \quad (40)$$

Note that $\det[B_2(x)] = \frac{1}{L_d L_q} \neq 0$, thus $B_2(x)$ is nonsingular in all the feasible zone. In other words, above input-output linearization is valid.

Define perturbation $\psi_2(\cdot)$ and $\psi_3(\cdot)$ to describe the nonlinearities and uncertainties of $F_2(x)$, $F_3(x)$, and $B_2(x)$, yields

$$\begin{bmatrix} \psi_2(\cdot) \\ \psi_3(\cdot) \end{bmatrix} = \begin{bmatrix} F_2(x) \\ F_3(x) \end{bmatrix} + (B_2(x) - B_2(0)) \begin{bmatrix} u_2(x) \\ u_3(x) \end{bmatrix} \quad (41)$$

where $B_2(0) = \begin{bmatrix} b_{20} & 0 \\ 0 & b_{30} \end{bmatrix}$ is constant control gain.

Define tracking error $e = [e_2 \quad e_3]^T = [i_d - i_d^*, i_q - i_q^*]^T$, one can obtain

$$\begin{bmatrix} \dot{e}_2 \\ \dot{e}_3 \end{bmatrix} = \begin{bmatrix} \psi_2(\cdot) \\ \psi_3(\cdot) \end{bmatrix} + B_2(0) \begin{bmatrix} u_2 \\ u_3 \end{bmatrix} \quad (42)$$

Then, two second order sliding-mode perturbation observers (SMPOs) are adopted to estimate $\psi_2(\cdot)$ and $\psi_3(\cdot)$, as

$$\begin{cases} \dot{\hat{i}}_d = \hat{\psi}_2(\cdot) + \alpha_{21} \tilde{i}_d + k_{21} \text{sat}(\tilde{i}_d, \delta_{o2}) + b_{20} u_2 \\ \hat{\psi}_2(\cdot) = \alpha_{22} \tilde{i}_d + k_{22} \text{sat}(\tilde{i}_d, \delta_{o2}) \end{cases} \quad (43)$$

$$\begin{cases} \dot{\hat{i}}_q = \hat{\psi}_3(\cdot) + \alpha_{31} \tilde{i}_q + k_{31} \text{sat}(\tilde{i}_q, \delta_{o2}) + b_{30} u_3 \\ \hat{\psi}_3(\cdot) = \alpha_{32} \tilde{i}_q + k_{32} \text{sat}(\tilde{i}_q, \delta_{o2}) \end{cases} \quad (44)$$

where positive constants α_{21} , α_{22} , α_{31} , α_{32} , k_{21} , k_{22} , k_{31} and k_{32} are observer gains.

The estimated sliding surface of system (37) is chosen as

$$\begin{bmatrix} \hat{S}_2 \\ \hat{S}_3 \end{bmatrix} = \begin{bmatrix} \hat{i}_d - i_d^* \\ \hat{i}_q - i_q^* \end{bmatrix} \quad (45)$$

Finally, the POSMC of system (37) is designed as

$$\begin{bmatrix} u_2 \\ u_3 \end{bmatrix} = \frac{1}{B_2(0)} \begin{bmatrix} \dot{i}_d^* - \varsigma_2 \hat{S}_2 - \varphi_2 \text{sat}(\hat{S}_2, \partial c_2) - \hat{\psi}_2(\cdot) \\ \dot{i}_q^* - \varsigma_3 \hat{S}_3 - \varphi_3 \text{sat}(\hat{S}_3, \partial c_2) - \hat{\psi}_3(\cdot) \end{bmatrix} \quad (46)$$

where $\varsigma_1, \varsigma_2, \varphi_1,$ and φ_2 are controller gains.

At this end, the overall block diagram of POSMC is shown in Fig. 3.

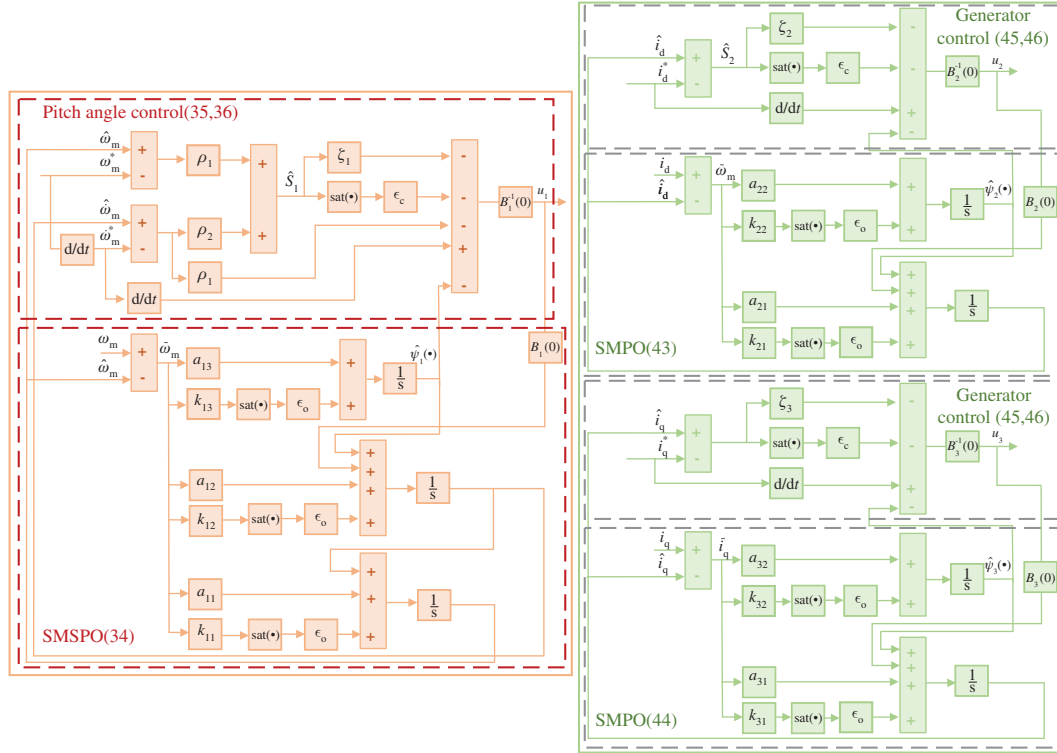


Figure 3: The overall block diagram of POSMC

4.4 Analysis and Discussion

As described in Assumption 2, the perturbation and its derivative are locally bounded. And the deduction of these bounds is given as

$$\begin{aligned} \psi_1(\cdot) &= F_1(x) + \left(\frac{B_1(x) - B_1(0)}{B_1(x)} \right) [-\rho_1(\hat{\omega}_m - \dot{\omega}_m^*) - \varsigma_1 \hat{S}_1 - \varphi_1 \text{sat}(\hat{S}_1, \partial c) + \ddot{\omega}_m^* - \hat{\psi}_1(\cdot)] \\ &= F_1(x) + \left(\frac{B_1(x) - B_1(0)}{B_1(x)} \right) [-\rho_1 e_{11} - \varsigma_1 \hat{S}_1 - \varphi_1 \text{sat}(\hat{S}_1, \partial c) + \varepsilon_{11}] \end{aligned} \quad (47)$$

$$\begin{aligned} \psi_2(\cdot) &= F_2(x) + \left(\frac{B_{21}(x) - B_{21}(0)}{B_{21}(x)} \right) (-\varsigma_2 \hat{S}_2 - \varphi_2 \text{sat}(\hat{S}_2, \partial c_2) + \dot{i}_d^* - \hat{\psi}_2(\cdot)) \\ &= F_2(x) + \left(\frac{B_{21}(x) - B_{21}(0)}{B_{21}(x)} \right) (-\varsigma_2 \hat{S}_2 - \varphi_2 \text{sat}(\hat{S}_2, \partial c_2) + \varepsilon_{21}) \end{aligned} \quad (48)$$

$$\begin{aligned}\psi_3(\cdot) &= F_3(x) + \left(\frac{B_{24}(x) - B_{24}(0)}{B_{24}(x)}\right)(-\varsigma_3 \hat{S}_3 - \varphi_3 \text{sat}(\hat{S}_3, \dot{\delta}_{c2}) + i_q^* - \hat{\psi}_3(\cdot)) \\ &= F_3(x) + \left(\frac{B_{24}(x) - B_{24}(0)}{B_{24}(x)}\right)(-\varsigma_3 \hat{S}_3 - \varphi_3 \text{sat}(\hat{S}_3, \dot{\delta}_{c2}) + \varepsilon_{22})\end{aligned}\quad (49)$$

$$\dot{\psi}_1(\cdot) = \dot{F}_1(x) + \left(\frac{B_1(x) - B_1(0)}{B_1(0)}\right)(-\rho_1 \dot{e}_{11} - \varsigma_1 \dot{S}_1 - \varphi_1 \text{sat}(\dot{S}_1, \dot{\delta}_c) + \dot{\varepsilon}_{11}) \quad (50)$$

$$\dot{\psi}_2(\cdot) = \dot{F}_2(x) + \left(\frac{B_{21}(x) - B_{21}(0)}{B_{21}(0)}\right)(-\varsigma_2 \dot{S}_2 - \varphi_2 \text{sat}(\dot{S}_2, \dot{\delta}_{c2}) + \dot{\varepsilon}_{21}) \quad (51)$$

$$\dot{\psi}_3(\cdot) = \dot{F}_3(x) + \left(\frac{B_{24}(x) - B_{24}(0)}{B_{24}(0)}\right)(-\varsigma_3 \dot{S}_3 - \varphi_3 \text{sat}(\dot{S}_3, \dot{\delta}_{c2}) + \dot{\varepsilon}_{22}) \quad (52)$$

$$|\psi_1| \leq \frac{1}{1 - \theta_1} |F_1(x)| + \frac{\theta_1}{1 + \theta_1} (\|\rho_1\| \|e_{11}\| + \|\varsigma_1\| + \|\varphi_1\| + |\varepsilon_{11}|) \quad (53)$$

$$|\psi_2| \leq \frac{1}{1 - \theta_2} |F_2(x)| + \frac{\theta_2}{1 + \theta_2} (\|\varsigma_2\| + \|\varphi_2\| + |\varepsilon_{21}|) \quad (54)$$

$$|\psi_3| \leq \frac{1}{1 - \theta_3} |F_3(x)| + \frac{\theta_3}{1 + \theta_3} (\|\varsigma_3\| + \|\varphi_3\| + |\varepsilon_{22}|) \quad (55)$$

$$|\dot{\psi}_1| \leq |\dot{F}_1(x)| + |B_1(x)| \|u_1\| + \theta_1 (\|\rho_1\| \|\dot{e}_{11}\| + \|\varsigma_1\| + \|\varphi_1\| + |\dot{\varepsilon}_{11}|) \quad (56)$$

$$|\dot{\psi}_2| \leq |\dot{F}_2(x)| + |B_{21}(x)| \|u_2\| + \theta_2 (\|\varsigma_2\| + \|\varphi_2\| + |\dot{\varepsilon}_{21}|) \quad (57)$$

$$|\dot{\psi}_3| \leq |\dot{F}_3(x)| + |B_{24}(x)| \|u_3\| + \theta_3 (\|\varsigma_3\| + \|\varphi_3\| + |\dot{\varepsilon}_{22}|) \quad (58)$$

Hence, the validity of the developed perturbation observer is demonstrated.

5 Case Studies

Three cases, e.g., ramp wind speed, random wind speed, and parameter uncertainty, are undertaken to assess the performance of POSMC compared with that of VC [15], FLC [24], and NAC [14]. The simulation is implemented based on MATLAB R2019a by a desktop computer with an Intel® Core™ i5 CPU at 3.4 GHz and 16 GB of RAM. And the parameters of PMSG and POSMC are listed in Tabs. 1 and 2, respectively.

5.1 Ramp Wind Speed

A ramp wind signal changing from 18 m/s to 14 m/s is exerted to WECS, as shown in Fig. 4. The simulation outcomes of four controllers under ramp wind are shown in Fig. 5. One can easily find that VC has the longest convergence time and the biggest tracking error of ω_m due to its control gains are obtained by local linearization of specific system operating point. FLC has obvious oscillation of ω_m , P_m , and Q_m during running period which needs full state measurements. Meanwhile, NAC has the highest overshoot of i_{md} and i_{mq} compared with other three methods. And POSMC can obtain the satisfactory control performance with the fast convergence speed and the small tracking error. Specially, the convergence time of VC, FLC, NAC, and POSMC in terms of ω_m are 4.16 s, 5.71 s, 5.80 s, and 16.46 s, respectively. And the maximum overshoot of P_m of VC, FLC, NAC and POSMC is 8.70% and 3.55%, 1.25% and 0.15%, respectively. Meanwhile, the errors between the estimations and actual values of the designed observers are shown in Fig. 6 which provides satisfactory estimation.

Table 1: Parameters of PMSG

Parameters	Values	Units	Parameters	Values	Units
Actuator time constant τ_β	1	s	Air density ρ	1.205	kg/m ³
Blade radius R	39	m	d-axis inductance L_d	5.5	mH
d-axis stator current reference i_{mdr}	0	A	Field flux K_e	136.25	V·s/rad
Mechanical rotation speed reference	2.2489	rad/s	Number of pole pairs p	11	
Pitch angle rate β_{rate}	± 10	degree/s	q-axis inductance L_q	3.75	mH
q-axis stator current reference i_{mqr}	593.3789	A	Rated electromagnetic torque reference	889326.7	Nm
Rated output power P_r	2	MW	Rated wind speed V_r	12	m/s
Stator resistance R_s	50	$\mu\Omega$	Total inertia J_{tot}	10000	kg·m ²

Table 2: Parameters of POSMC

Pitch angle control	$\rho_1 = 1.4E3$ $k_{11} = 40$ $\alpha_{12} = 9.72E4$	$\rho_2 = 2$ $k_{12} = 3.2E3$ $\alpha_{13} = 5.832E6$	$\varsigma_1 = 18$ $k_{13} = 6.4E4$ $\delta_o = \delta_c = 0.1$	$\varphi_1 = 20$ $\alpha_{11} = 540$
Generator control	$\varsigma_2 = \varsigma_3 = 20$ $\alpha_{21} = \alpha_{31} = 2.8E3$	$\varphi_2 = \varphi_3 = 20$ $\alpha_{22} = \alpha_{32} = 2.0E6$	$k_{21} = k_{22} = 200$ $\delta_{o2} = \delta_{c2} = 0.2$	$k_{31} = k_{32} = 6.0E5$

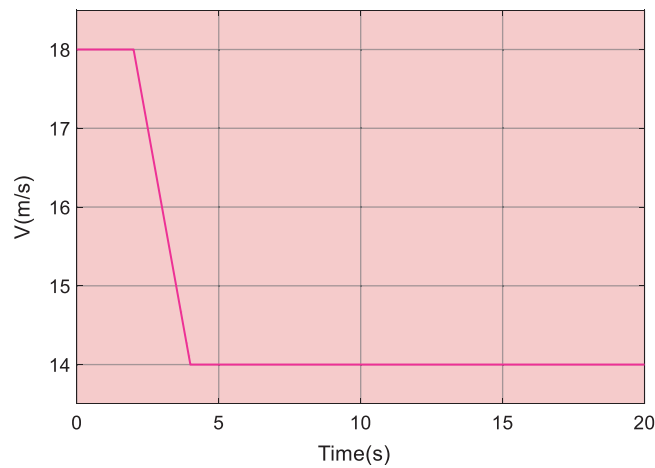


Figure 4: Ramp wind curve

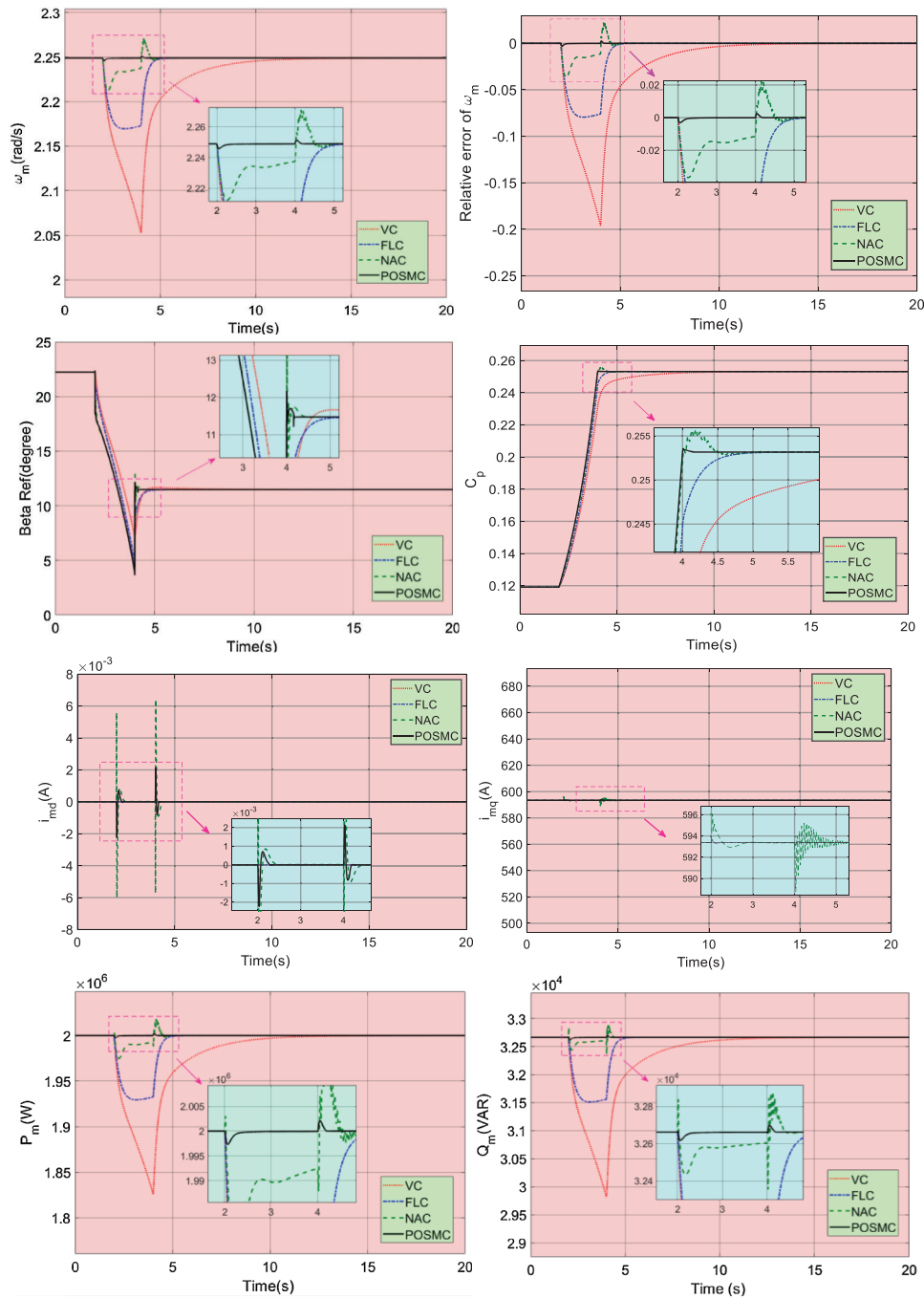


Figure 5: The simulation outcomes of four controllers under ramp wind speed

5.2 Random Wind Speed

The random wind curve is denoted in Fig. 7. And Fig. 8 describes the simulation outcomes under such scenario. Obviously, POSMC keeps ω_m , P_m and Q_m around their rated value during all the simulation time with the smallest overshoot and consistent control performance. Meanwhile, VC, FLC, and POSMC have the nearly similar control performance of i_{md} and i_{mq} . And Fig. 9 denotes the error between the estimations and actual values of the designed observers which prove that the developed SMSPO and SMPO have excellent tracking effects.

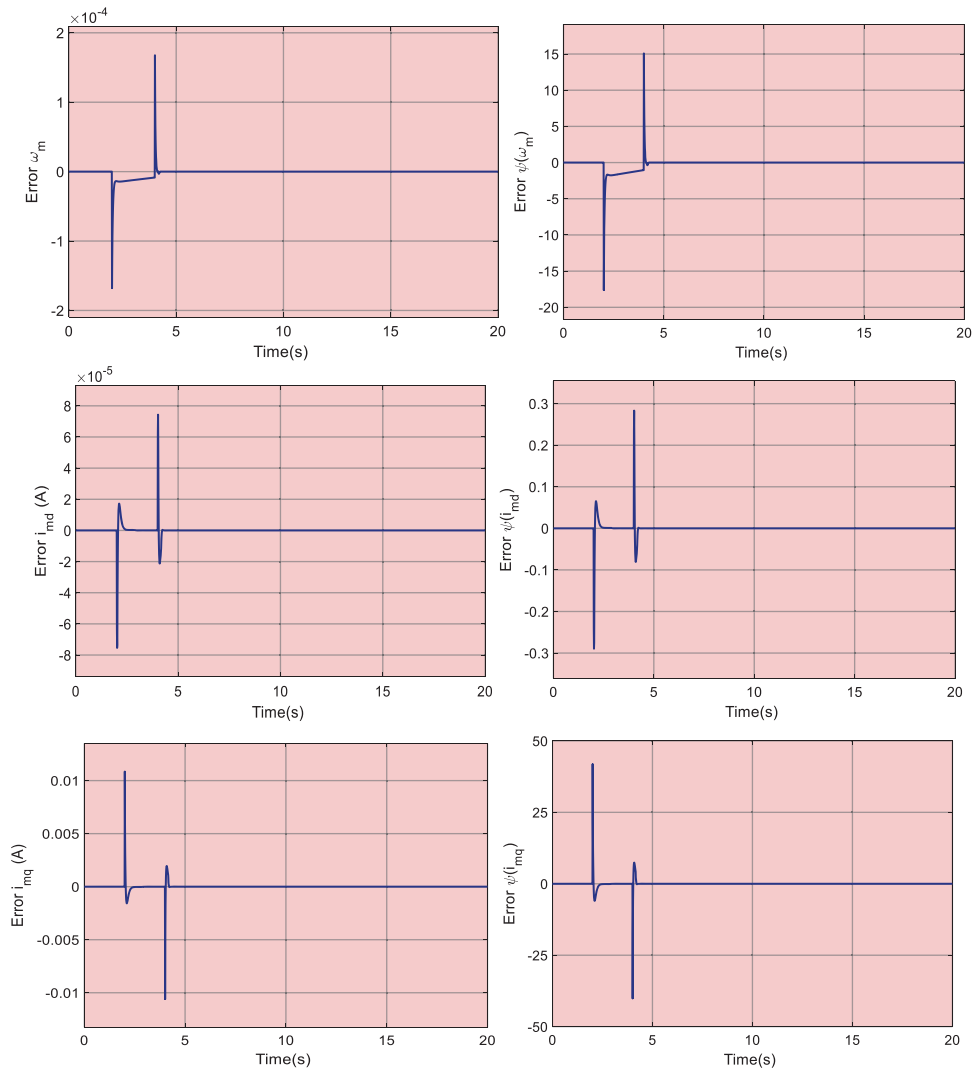


Figure 6: The error between the estimations and actual values of the designed observers under ramp wind speed

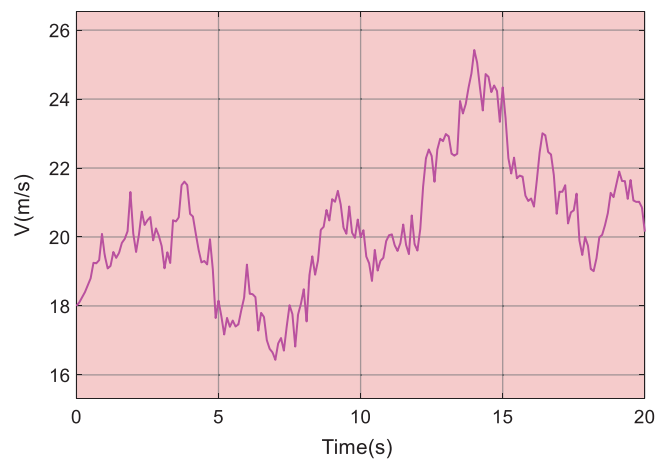


Figure 7: Random wind curve

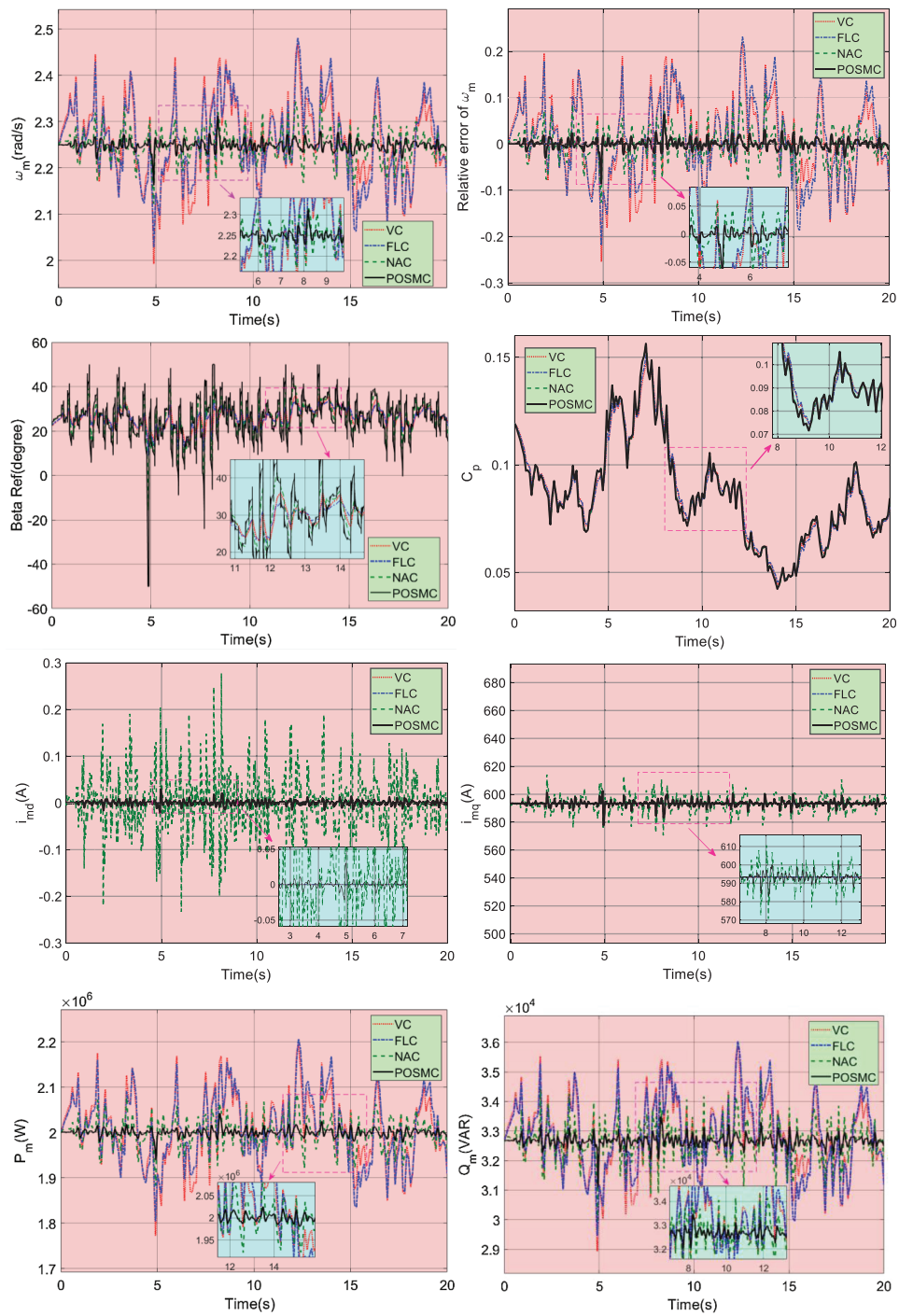


Figure 8: The simulation results of four controllers under random wind speed

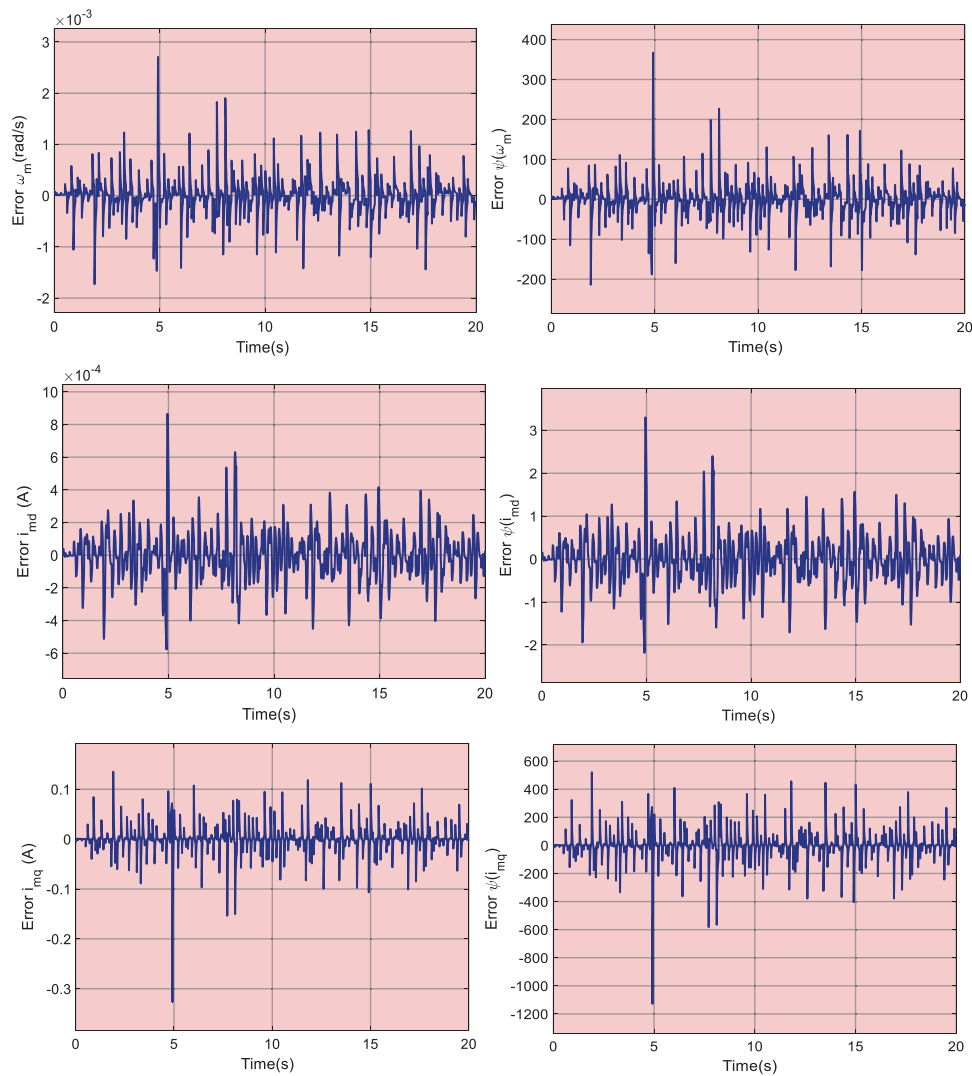


Figure 9: The error between the estimations and actual values of the designed observers under random wind speed

5.3 Parameter Uncertainty

In this case, the variation of field flux K_e from 1 (p.u.) at $t = 4s$ to 0.9 (p.u.) at $t = 9s$ is implemented to system for evaluating the robustness of four controllers. And wind speed remains at 18 m/s during all the simulation time. Fig. 10 shows the simulation outcomes of four controllers under above scenario. It is clear that POSMC can restore perturbed system with the fastest speed. Though VC and FLC have the lower oscillation of i_{md} because of the simple mechanism, they have the worst control performance in other seven output variables. And the maximum overshoot of ω_m of VC, FLC and NAC is 5.16% and 1.24% and 0.36%, respectively. While POSMC can realize nearly smooth tracking performance of all output variables with the strongest robustness.

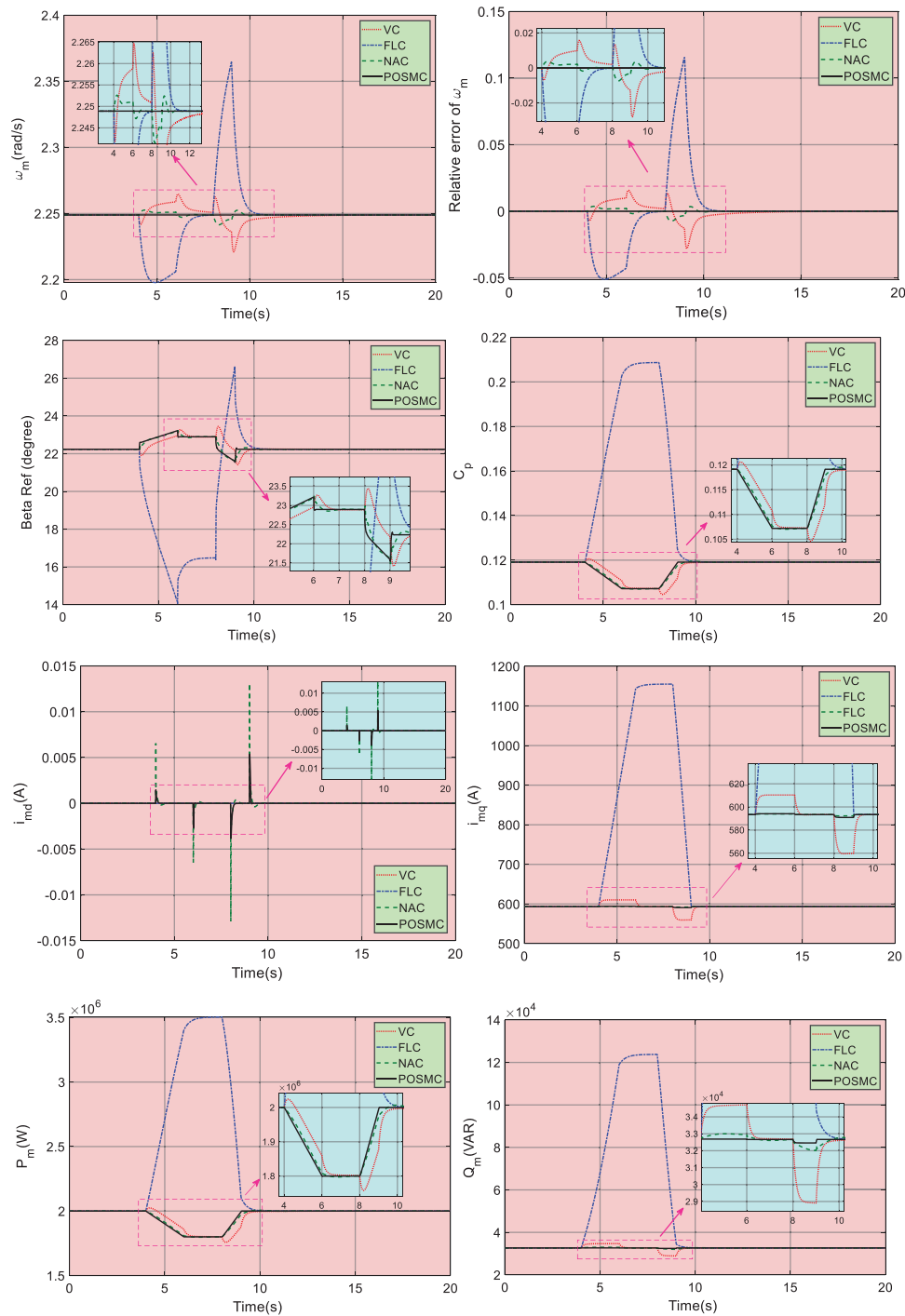


Figure 10: The simulation outcomes of four controllers under parameter uncertainty

5.4 Statistical Analysis

Integral absolute error index $IAE_x = \int_0^T |x - x^*| dt$ is widely used in the quantitative analysis of control errors, which describes the error accumulation of system output compared to its reference value over a period of time T . Tab. 3 gives IAE_{ω_m} , IAE_{i_d} , and IAE_{i_q} of four controllers in three cases. VC obtains the smallest

IAE i_d and IAE i_q in most cases thanks to its simple structure, but it has the longest recovery time and most obvious oscillations of ω_m due to the linear frame. And POSMC can obtain the smallest IAE ω_m in all the four controllers under three cases. Moreover, the overall control costs $\int_0^T (|\beta_r| + |V_d| + |V_q|)dt$ of four controllers are shown in Fig. 11. Although VC have the lower control costs than POSMC in ramp wind, it has poor control performance. While POSMC has the smallest control costs than VC, FLC, and NAC in random wind due to the integration of nonlinear real-time perturbation estimation and robust SMC structure. Specially, the overall control costs of POSMC are 99.58%, 99.52% and 96.73% of that of VC, FLC, and NAC in random wind.

Table 3: IAE indexes of four control approaches obtained in three scenarios (p.u.)

Scenario	IAE index	Controller			
		VC	FLC	NAC	POSMC
Ramp wind	IAE ω_m (rad)	0.4137	0.1555	4.312E-2	6.237E-4
	IAE i_d (A.s)	9.727E-15	1.025E-13	1.506E-2	2.84E-4
	IAE i_q (A.s)	8.554E-13	6.97E-12	3.196E-2	2.753E-2
Random wind	IAE ω_m (rad)	1.317	1.273	1.017	0.154
	IAE i_d (A.s)	1.003E-14	1.075E-13	7.848E-2	7.295E-2
	IAE i_q (A.s)	9.604E-13	7.155E-12	7.655E-2	2.436E-2
Parameter uncertainty	IAE ω_m (rad)	5.284E-2	0.207	2.742E-3	4.919E-5
	IAE i_d (A.s)	9.469E-15	1.24E-13	1.32E-3	7.168E-4
	IAE i_q (A.s)	67.7	1957	0.2213	0.1841

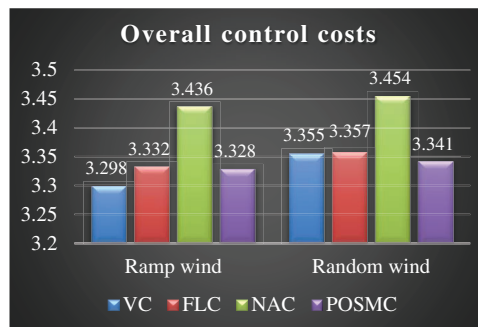


Figure 11: The overall control costs of four control approaches

6 Conclusions

In this paper, POSMC is applied in variable-pitch control of PMSG to limit generator’s output power at its rated value when the wind speed is higher than rated value. The main novelties/contributions can be concluded as follows:

- (i) POSMC combines nonlinearities, parametric uncertainties, unmodelled dynamics, and time-varying external disturbances into a new perturbation estimating via the perturbation observer. Subsequently, sliding mode control is designed to completely make up for the perturbation estimation in real-time for the sake of realizing a global consistent control performance and improving the robustness of the system under various operation conditions.

(ii) Compared with VC, POSMC is designed based on nonlinear architecture which is not affected by the changed system operating points.

(iii) Compared with FLC, POSMC only requires the measurements of d-q axis current and mechanical rotation speed ω_m rather than full-state measurements which are easy to implement.

(iv) Compared with NAC, POSMC has the better control performance in ramp wind and random wind, the higher robustness in terms of parameter uncertainty, the smaller IAE indexes and overall control costs. Specially, the IAE ω_m of POSMC is only 1.45%, 15.14% and 1.79% of that of NAC in ramp wind, random wind and parameter uncertainty, respectively. And the overall control costs of POSMC are 96.86% and 96.73% of that of NAC in ramp wind and random wind, respectively.

Future studies will be focused on carrying out the HIL experiment of variable-pitch PMSG to further prove the implementation feasibility of POSMC.

Funding Statement: The authors thankfully acknowledge the support of the Noise problem of electric vehicle brushless DC motor starting (S202010641109).

Conflicts of Interest: The authors declare that they have no conflicts of interest to report regarding the present study.

References

1. Xi, L., Chen, J., Huang, Y., Xu, Y. Liu, L. et al. (2018). Smart generation control based on multi-agent reinforcement learning with the idea of the time tunnel. *Energy*, 153, 977–987. DOI 10.1016/j.energy.2018.04.042.
2. Zhang, S. X., Yu, T., Yang, B., Li, L. (2016). Virtual generation tribe based robust collaborative consensus algorithm for dynamic generation command dispatch optimization of smart grid. *Energy*, 101, 34–51. DOI 10.1016/j.energy.2016.02.009.
3. Bani-Hani, E., Sedaghat, A., Saleh, A., Ghulom, A., Al-Rahmani, H. et al. (2019). Evaluating performance of horizontal axis double rotor wind turbines. *Energy Engineering*, 116(1), 26–40. DOI 10.1080/01998595.2019.12043336.
4. Peng, X. T., Yao, W., Yan, C., Wen, J. Y., Cheng, S. J. (2019). Two-stage variable proportion coefficient based frequency support of grid-connected DFIG-WTs. *IEEE Transactions on Power Systems*, 35(2), 962–974. DOI 10.1109/TPWRS.2019.2943520.
5. Yang, B., Zhong, L. E., Zhang, X. S., Shu, H. C., Yu, T. et al. (2019). Novel bio-inspired memetic salp swarm algorithm and application to MPPT for PV systems considering partial shading condition. *Journal of Cleaner Production*, 215, 1203–1222. DOI 10.1016/j.jclepro.2019.01.150.
6. Moya, D., Aldás, C., Kaparaju, P. (2018). Geothermal energy: Power plant technology and direct heat applications. *Renewable and Sustainable Energy Reviews*, 94, 889–901. DOI 10.1016/j.rser.2018.06.047.
7. Wu, J. M., Yao, Y. X., Li, W., Zhou, L., Goteman, M. (2017). Optimizing the performance of solo Duck wave energy converter in tide. *Energies*, 10(3), 289. DOI 10.3390/en10030289.
8. Ulazia, A., Penalba, M., Ibarra-Berastegui, G., Ringwood, J., Saenz, J. (2019). Reduction of the capture width of wave energy converters due to long-term seasonal wave energy trends. *Renewable and Sustainable Energy Reviews*, 113, 109267. DOI 10.1016/j.rser.2019.109267.
9. Badal, F. R., Das, P., Sarker, S. K., Das, S. J. (2019). A survey on control issues in renewable energy integration and microgrid. *Protection and Control of Modern Power Systems*, 4(1), 8. DOI 10.1186/s41601-019-0122-8.
10. Ayodele, T. R., Ogunjuyigbe, A. S. O., Olarewaju, R. O., Munda, J. L. (2019). Comparative assessment of wind speed predictive capability of first-and second-order markov chain at different time horizons for wind power application. *Energy Engineering*, 116(3), 54–80. DOI 10.1080/01998595.2019.12057062.
11. Global Wind Energy Council (2019). Global Wind Report 2019. <https://gwec.net/global-wind-report-2019>.
12. Wang, Y. F., Zhao, C. Y., Guo, C. Y., Rehman, A. U. (2020). Dynamics and small signal stability analysis of PMSG-based wind farm with an MMC-HVDC system. *CSEE Journal of Power and Energy Systems*, 6(1), 226–235.

13. Alsumiri, M., Li, L. Y., Jiang, L., Tang, W. H. (2018). Residue Theorem based soft sliding mode control for wind power generation systems. *Protection and Control of Modern Power Systems*, 3(1), 24. DOI 10.1186/s41601-018-0097-x.
14. Chen, J., Yang, B., Duan, W. Y., Shu, H. C., An, N. et al. (2019). Adaptive pitch control of variable-pitch PMSG based wind turbine. *Applied Sciences*, 9(19), 4109. DOI 10.3390/app9194109.
15. Yang, B., Yu, T., Shu, H. C., Jiang, L. (2018). Robust sliding-mode control of wind energy conversion systems for optimal power extraction via nonlinear perturbation observers. *Applied Energy*, 210, 711–723. DOI 10.1016/j.apenergy.2017.08.027.
16. Yang, B., Yu, T., Shu, H. C., Zhang, Y. M., Chen, J. et al. (2018). Passivity-based sliding-mode control design for optimal power extraction of a PMSG based variable speed wind turbine. *Renewable Energy*, 119, 577–589. DOI 10.1016/j.renene.2017.12.047.
17. Shaked, U., Soroka, E. (1985). On the stability robustness of the continuous-time LQG optimal control. *IEEE Transactions on Automatic Control*, 30(10), 1039–1043. DOI 10.1109/TAC.1985.1103811.
18. Guchhait, P. K., Banerjee, A. (2020). Stability enhancement of wind energy integrated hybrid system with the help of static synchronous compensator and symbiosis organisms search algorithm. *Protection and Control of Modern Power Systems*, 5(1), 11. DOI 10.1186/s41601-020-00158-8.
19. Kim, J., Jeon, J., Heo, H. (2011). Design of adaptive PID for pitch control of large wind turbine generator. *10th International Conference on Environment and Electrical Engineering*. Rome, Italy.
20. Dou, Z. L., Cheng, M. Z., Ling, Z. B., Cai, X. (2010). An adjustable pitch control system in a large wind turbine based on a fuzzy-PID controller. *SPEEDAM 2010*, pp. 391–395. Pisa, Italy.
21. Zhang, X. S., Li, Q., Yu, T., Yang, B. (2018). Consensus transfer Q-learning for decentralized generation command dispatch based on virtual generation tribe. *IEEE Transactions on Smart Grid*, 9(3), 2152–2165.
22. Senjyu, T., Sakamoto, R., Urasaki, N., Funabashi, T., Fujita, H. et al. (2006). Output power leveling of wind turbine generator for all operating regions by pitch angle control. *IEEE Transactions on Energy Conversion*, 21(2), 467–475. DOI 10.1109/TEC.2006.874253.
23. Van, T. L., Nguyen, T. H., Lee., D. (2015). Advanced pitch angle control based on fuzzy logic for variable-speed wind turbine systems. *IEEE Transactions on Energy Conversion*, 30(2), 578–587. DOI 10.1109/TEC.2014.2379293.
24. Wang, C. S., Chiang, M. H. (2016). A novel pitch control system of a large wind turbine using two-degree-of-freedom motion control with feedback linearization control. *Energies*, 9(10), 791. DOI 10.3390/en9100791.
25. Yilmaz, A. S., Özer, Z. (2009). Pitch angle control in wind turbines above the rated wind speed by multi-layer perceptron and radial basis function neural networks. *Expert Systems with Applications*, 36(6), 9767–9775. DOI 10.1016/j.eswa.2009.02.014.
26. Yang, B., Zhong, L. E., Yu, T. Shu, Cao, H. C., An, P. L. et al. (2019). PCSMC design of permanent magnetic synchronous generator for maximum power point tracking. *IET Generation, Transmission & Distribution*, 13(14), 3115–3126. DOI 10.1049/iet-gtd.2018.5351.
27. Yang, B., Yu, T., Shu, H. C., Zhu, D. N., Sang, Y. Y. et al. (2018). Perturbation observer based fractional-order sliding-mode controller for MPPT of grid-connected PV inverters: Design and real-time implementation. *Control Engineering Practice*, 79, 105–112. DOI 10.1016/j.conengprac.2018.07.007.
28. Yang, B., Sang, Y. Y., Shi, K., Jiang, L., Yu, T. (2016). Design and real-time implementation of perturbation observer based sliding-mode control for VSC-HVDC systems. *Control Engineering Practice*, 56, 13–26. DOI 10.1016/j.conengprac.2016.07.013.
29. Kwon, S. J., Chung, W. K. (2003). A discrete-time design and analysis of perturbation observer for motion control applications. *IEEE Transactions on Control Systems Technology*, 11(3), 399–407. DOI 10.1109/TCST.2003.810398.
30. Chen, J., Jiang, L., Yao, W., Wu, Q. H. (2013). A feedback linearization control strategy for maximum power point tracking of a PMSG based wind turbine. *International Conference on Renewable Energy Research and Applications (ICRERA)*, pp. 79–84. Madrid, Spain.